ChemComm

Accepted Manuscript

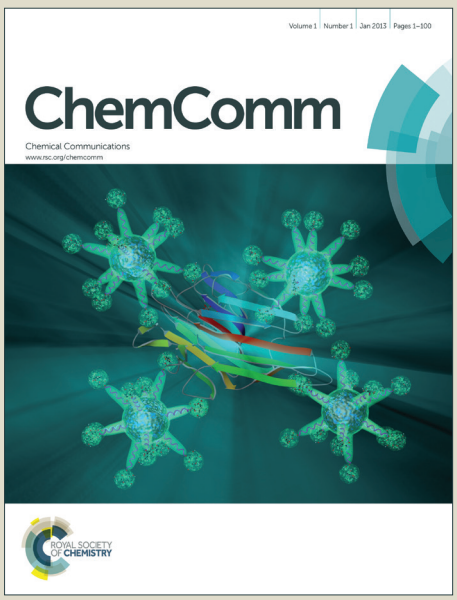

ROYAL SOCIETY OF CHEMISTRY

www.rsc.org/chemcomm

Cite this: DOI: 10.1039/c0xx00000x

www.rsc.org/xxxxxx

Communication

7.35%−Efficiency rear−irradiated flexible dye−sensitized solar cell by sealing liquid electrolyte in a groove

Xiaopeng Wang,[a,b,c] Qunwei Tang,*[a,b,c] Benlin He,[b] Ru Li [a] and Liangmin Yu*[a,c]

Received (in XXX, XXX) Xth XXXXXXXXX 20XX, Accepted Xth XXXXXXXXX 20XX

DOI: 10.1039/b000000x

We present here the feasibility of assembling rear−irradiated flexible dye−sensitized solar cell employing transparent Ni−Se alloy counter electrode along with groove stored TiO_2 and liquid electrolyte. The flexible device with NiSe counter electrode and anode at a groove depth of 36 μm yields a maximum efficiency of 7.35%.

Dye−sensitized solar cell (DSSC) is an electrochemical device converting solar energy into electricity with no emissions.[1−7] The state−of−the−art DSSCs are always assembled on fluorine−doped tin oxide (FTO) conductive glass substrates,[8,9] leading to inferiorities in frangibility, high weight, unyieldingness, and high cost. One solution to this impasse is the employment of flexible substrates such as Ti foil,[10] tin doped indium oxide (ITO)/poly(ethylene naphthalate) (PEN),[11] or ITO/poly(ethylene terephthalate) (PET) substrates for flexible DSSC assembly. Due to a fact that the ITO/PEN or ITO/PET substrates suffer devitrification and deformation at calcination temperature exceeding 150 ºC, therefore, conductive plastic supported TiO_2 can not realize the crystal transition from rutile to anatase. That is not suprising to obtain unsatisfactory power conversion efficiencies from flexible cell devices.[12−14] Although there are emerging low−temperature techniques for anatase TiO_2 nanocrystallites,[15] the adhesiveness between TiO_2 film and flexible substrate is still unsatisfactory, leading to a high interfacial resistance for electron transportation. An ideal flexible DSSC comprises a Ti foil supported TiO_2 anode, Pt coated ITO/PEN (or ITO/PET) counter electrode (CE), and liquid electrolyte containing I^-/I_3^- redox couples. Viewed from this point, irradiation from rear side is the sole technique for driving this system.[16] However, traditional Pt CE has metallic luster and therefore can reflect most of incident light, resulting in a low light intensity for dye irradiation and electron generation. Another remaining problem is the leakage and evaporation of liquid electrolyte. Although the utilization of quasi−solid−state and full−solid−state electrolytes can well reserve redox couples,[17−20] the relatively low charger transfer kinetics within the electrolytes has been considered a tremendous limit for efficiency enhancement. By addressing these two issues, the explorations of cost−effective and transparent CEs as well as a new sealing strategy for liquid electrolyte seem to be crucial for achieving cell devices with high efficiency and good stability.

Inspired by a container for liquid storage, in which the bottom and surrounding sides are blocked, leaving top cover open, in the current work, we have successfully designed transparent nickel selenide (Ni−Se) alloys on flexible ITO/PEN substrates and etching of Ti foil for reserving dye−sensitized TiO_2 and liquid electrolyte. The TiO_2 film is consolidated within the etched groove and liquid electrolyte is stored in the nanopores of TiO_2 layer. Therefore, the leakage issue for liquid electrolyte can be well solved by sealing it in a groove surrounded by Ti foil and Ni−Se CE cover in comparison with interface sealing in a traditional flexible DSSC device. A maximum efficiency of 7.35% is recorded under simulated air mass 1.5 (AM1.5) global sunlight by optimizing Ni/Se ratio and groove depth.

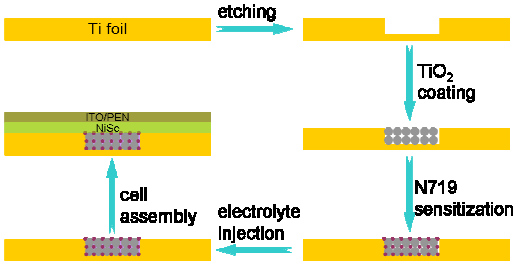

Fig. 1 Schematic diagram for the flexible DSSC device comprising of ITO/PEN supported Ni−Se alloy and Ti foil reserved liquid electrolyte and dye−sensitized TiO_2.

Fig. 1 presents schematic diagram of processes for etching, TiO_2 coating, dye sensitization, electrolyte injection, and cell assembly. The depth of the groove is controlled by adjusting etching time. In the current work an etching speed of 3 μm cm^{-1} is utilized to creat grooves. Like a container, the injected liquid electrolyte is reserved by etched groove and covered by Ni−Se alloy electrode.

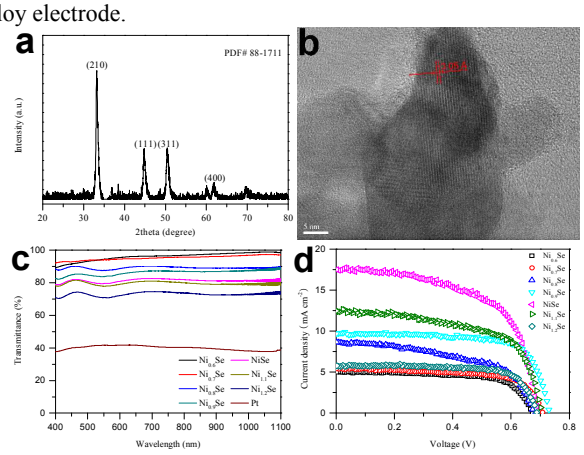

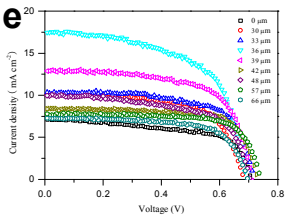

Fig. 2 (a) XRD pattern and (b) TEM photograph of NiSe alloy electrode. (c) Optical transmission of various CEs and (d) characteristic *J*−*V* curves for their DSSCs with a groove depth of 36 μm. (e) Characteristic *J*−*V* curves for the cells with NiSe CE and anodes at various groove depths.

As shwon in Fig. 2a, X−ray diffraction (XRD) gives characteric diffraction peaks at 2θ = 33.2º, 44.7º, 50.5º, and 61.8º for (210), (111), (311), and (400) facets, respectively. The result indicates that NiSe alloy (PDF#88−1711) has been successfully synthesized by the electrochemical deposition reported here. Lattice fringes can be observed in high−resolution transmission electron microscopy (HRTEM) photograph, as shown in Fig. 2b, suggesting that the resultant alloy has a good crystallinity. Moreover, the detection of lattice distortions reveals the formation of defects by alloying Ni and Se, promoting the I_3^- reduction process. As shown in Fig. 2c, the resultant flexible Ni−Se alloy electrodes have high optical transparency in visible region (> 70%), suggesting a good dye excitation and electron generation at rear irradiation.[21] Fig. 2d compares *J*−*V* curves of the DSSCs employing various CEs irradiated from rear side and the detailed photovoltaic parameters are summarized in Table S1. The cell device with NiSe alloy CE yields an η of 7.35% (J_{sc} = 17.52 mA cm^{-2}, V_{oc} of 0.69 V, and *FF* of 60.8%) under simulated AM1.5, which is superior to the flexible DSSCs in literatures.[22−24] Ni is a typical transition metal, having unfilled valence in *d* orbital. Therefore, the alloying of Ni with Se can accept electrons to form coordinated intermediates, which is a prerequisite for robust CE materials. Due to a fact of having remarkable catalytic activities for Se and Ni, they have been widely used as electrocatalysts in driving fuel cells.[25,26] To our knowledge, the measured η is in a very high level for liquid electrolyte based flexible DSSCs with Pt−free CEs. The η follows an order of NiSe > $Ni_{1.1}Se$ > $Ni_{0.9}Se$ > $Ni_{0.8}Se$ > $Ni_{1.2}Se$ > $Ni_{0.7}Se$ > $Ni_{0.6}Se$ because of a synergistic effect of catalytic activity, charge−transfer ability, and transparency. In order to investigate the dependence of TiO_2 thickness on photovoltaic performances, the Ti foil has been etched to obtain various groove depths with a range of 0 ~ 66 μm. Fig. 2e exhibits the characteristic *J*−*V* curves of cell devices with FeSe CE and anodes at diverse TiO_2 film thickness. Different from traditional DSSCs, the incident light penetrate into the cell device from rear side (CE side), therefore thick TiO_2 is expected to increase N719 dye loading. From Table S2, it is apparent that the J_{sc} has a peak value at TiO_2 thickness of 36 μm (Fig. S1). The elevated dye loading and therefore photogenerated electrons density on conduction band of TiO_2 have a promotion on J_{sc} in a thickness range of 0 ~ 36 μm. However, a much higher TiO_2 thickness such as higher than 36 μm can cause two issues: (i) no light irradiation for adsorbed N719 dyes in the deep, (ii) the diffusion of I_3^- species to groove bottom. A direct result is the decrease of interconversion between I_3^- and I^- and therefore dye recovery kinetics. If not specified, the thickness of TiO_2 layer is 36 μm. As a reference, the ITO/PEN supported Pt electrode was also prepared by the same cyclic voltammetry method, giving a comparable η of 2.75% (J_{sc} = 6.03 mA cm^{-2}, V_{oc} of 0.682 V, and *FF* of 66.9%), as shwon in Fig. S2a. The low power conversion efficiency is mainly attributed to the high reflection toward incident light (Fig. 2c) because the pristine Pt electrode has similar catalytic activity with $Ni_{0.8}Se$ alloy CE (Fig. S2b and Fig. S2c).

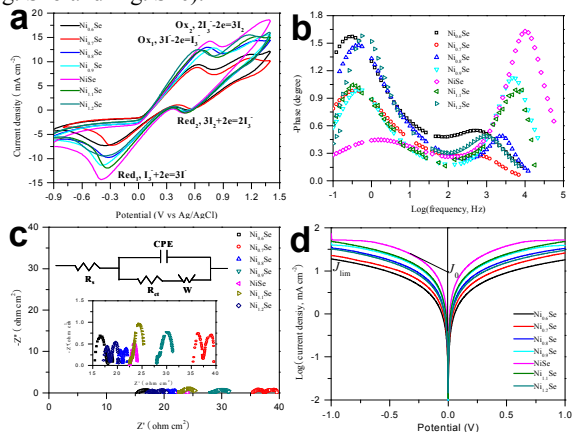

Fig. 3 (a) CV curves of various CEs for I^-/I_3^- redox species recorded at a scan rate of 50 mV s^{-1}. (b) Bode and (c) Nyquist EIS plots and (d) Tafel polarization curves of the symmetric dummy cells from two identical CEs. The insets show magnified Nyquist EIS plots and an equivalent circuit.

A golden rule in evaluating the function of a CE for DSSC application is to compare catalytic activity for the reduction of I_3^- ions. Fig. 3a displays cyclic voltammogram (CV) curves of Ni−Se alloy electrodes recorded at a scan rate of 50 mV s^{-1}, giving two pairs of oxidation/reduction peaks (Ox_1/Red_1, Ox_2/Red_2). The peak current density of Red_1 and Ox_1/|Red_1| ratio are two key parameters for assessing the catalytic activity and reversiblity of a CE toward I^-/I_3^- redox couples.[27] Due to a fact that the Red_1 peaks have similar positions, therefore the catalytic activities of alloy electrodes are NiSe > $Ni_{1.1}Se$ > $Ni_{0.9}Se$ > $Ni_{0.8}Se$ > $Ni_{1.2}Se$ > $Ni_{0.7}Se$ > $Ni_{0.6}Se$. From the outward extension of the peak positions in stacking CV curves of NiSe alloy electrode along with linear relationships between square root of scan rate and peak current densities, as shown in Fig. S3, we can conclude that the redox reaction is a diffusion−controlled mechanism on alloy CE.[28] From the Red_1 peak current density (J_{red1}), we can obtain diffusion coefficient (D_n) of I^-/I_3^- redox couples at electrode surface by Randles−Sevcik theory (J_{red1} = $2.69 \times 10^5 n^{3/2} A D_n^{1/2} v^{1/2} C$):[29−32] NiSe ($2.82 \times 10^{-6}$ cm^{-2} s^{-1}) > $Ni_{1.1}Se$ (1.97×10^{-6} cm^{-2} s^{-1}) > $Ni_{0.9}Se$ (1.80×10^{-6} cm^{-2} s^{-1}) > $Ni_{0.8}Se$ (1.31×10^{-6} cm^{-2} s^{-1}) > $Ni_{1.2}Se$ (1.25×10^{-6} cm^{-2} s^{-1}) > $Ni_{0.7}Se$ (7.42×10^{-7} cm^{-2} s^{-1}) > $Ni_{0.6}Se$ (7.29×10^{-7} cm^{-2} s^{-1}), where *n* is number of electron participating in Red_1 reaction, *A* is active area, *v* is scan rate, and *C* is I_3^- concentration. Notably, Ox_1/|Red_1| of alloy electrodes are calculated to be 0.995 for NiSe, 1.03 for $Ni_{1.1}Se$, 1.12 for $Ni_{0.9}Se$, 1.21 for $Ni_{0.8}Se$, 1.28 for $Ni_{1.2}Se$, 1.30 for $Ni_{0.7}Se$, and 1.32 for $Ni_{0.6}Se$. Higher peak current density and D_n along with lower Ox_1/|Red_1| suggest that the NiSe alloy CE presents higher catalytic activity and better reversiblity,[33] which are paramount prerequisites for a robust CE in efficient DSSC. Bode EIS plots from symmetric dummy cells in Fig. 3b provides direct evidence to calculate the average reduction time of I_3^- species. The electrons collected by alloy CE

from external circuit participate in reduction reaction of I_3^- + 2e → 3I^-, therefore lifetime (τ) of the electrons at electrolyte/CE interface can be utilized to assess the reaction kinetics of CE material. The electron lifetime can be obtained by $\tau = 1/2\pi f$, [34] giving average electron lifetime of NiSe (15.9 μs) < $Ni_{1.1}Se$ (19.1 μs) < $Ni_{0.9}Se$ (34.0 μs) < $Ni_{0.8}Se$ (61.9 μs) < $Ni_{1.2}Se$ (155.5 μs) < $Ni_{0.7}Se$ (235.4 μs) < $Ni_{0.6}Se$ (289.6 μs), where f is frequency of the second peak. A short τ means that the reflux electrons (from external circuit to CE) can be facilely collected by alloy film and are involved in the I_3^- reduction reaction (I_3^- + 2e$^-$ → 3I^-). To demonstrate the charge−transfer ability of alloy electrodes, Nyquist electrochemical impedance spectra (EIS) spectra in Fig. 3c are recording in symmetric dummy cells. After being fitted by Zview software, the related charge−transfer resistances (R_{ct}) obeys an order of NiSe (0.21 Ω cm^2) < $Ni_{1.1}Se$ (0.35 Ω cm^2) < $Ni_{0.9}Se$ (0.37 Ω cm^2) < $Ni_{0.8}Se$ (1.07 Ω cm^2) < $Ni_{1.2}Se$ (1.52 Ω cm^2) < $Ni_{0.7}Se$ (2.10 Ω cm^2) < $Ni_{0.6}Se$ (2.74 Ω cm^2). Tafel polarization measurements are utilized to reconfirm the catalytic activity and charger−transfer ability of the metal selenide alloy electrodes. As shown in Fig. 3d, the exchange current density ($J_0 = RT/nFR_{ct}$) derived from the slopes for anodic or cathodic branches are in an order of NiSe > $Ni_{1.1}Se$ > $Ni_{0.9}Se$ > $Ni_{0.8}Se$ > $Ni_{1.2}Se$ > $Ni_{0.7}Se$ > $Ni_{0.6}Se$.[35] Additionally, the limiting diffusion current density ($J_{lim} = 2nFCD_n/l$) generated from the intersection of cathodic branch with Y−axis also has the same sequence to J_0.[36] Till now, we can make a conclusion that the results from CV curves, lifetime analysis, EIS spectra, and Tafel polarization measurements are highly consistent.

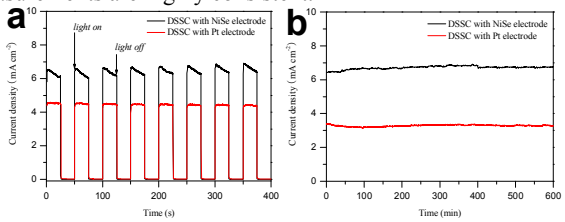

Fig. 4 (a) The start−stop switches and (b) photocurrent stability for the DSSC with NiSe alloy electrode and anode at a groove depth of 36 μm.

Fast start−up, multiple start/stop cycling, and high stability are three prerequisites for the applications of solar panels in movable power sources and photovoltaic curtain walls. A critical issue in solving these problems is to explore efficient electrocatalyst for CE.[37,38] Fig. 4a shows on−off (start−stop) switch on the cell with NiSe electrode by alternatively irradiating the device with intensities of 100 and 0 mW cm^{-2}. An abrupt increase in current density and no delay in time suggests that the resultant NiSe alloy CE is vigorous in reducing I_3^- species. As a reference, the related on−off switch of standard Pt electrode based DSSC is also provided, in which a lower current density means a lack of motivation in driving a DSSC. Additionally, start/stop cycling can be employed to evaluate the multilple start−up capability of a DSSC. After eight start/stop cycles, the cell still remain properties in its initial level, which is an essential prerequisite for the application of DSSCs in power sources. Under durable irradiation over 600 min, as shown in Fig. 4b, 101.3% and 99.8% of initial photocurrent densities are remained for the cells with NiSe and Pt electrodes, respectively. The result suggests relatively good stabilities for the solar cells with NiSe alloy and pristine Pt electrode, which is consistent with normalized efficiency in Fig. S4. Although the 600 min−test is far from to evaluate the long−term stability of a real cell device, the presented results demonstrate the potential realization of robust flexible DSSC reported here.

Conclusions

In summary, we have demonstrated that electrochemical deposition technique of Ni−Se alloys is an effective strategy for designing cost−effective and transparent CE materials and enhancing the photovoltaic performances of flexible DSSCs, whereas the seal of liquid electrolyte in etched groove of Ti foil can significantly enhance the electrolyte retention. NiSe alloy CE exhibits superior electrocatalytic activity toward I_3^- species and charge−transfer ability. The DSSC assembled by NiSe alloy CE and Ti foil reserved TiO_2 film with a thickness of 36 μm provides an impressive power conversion efficiency of 7.35% for irradiation from rear side. Moreover, the virtues on fast start−up, mutiple start/stop capability, and high stability motivate the potential applications of such flexible DSSCs in movable power sources and photovoltaic curtain walls. The research presented here is far from being optimized but the new concept along with cost−effective synthesis and scalable materials promise the CEs and anodes to be strong candidates in robust flexible DSSCs.

The authors gratefully acknowledge Fundamental Research Funds for the Central Universities (201313001, 201312005), Shandong Province Outstanding Youth Scientist Foundation Plan (BS2013CL015), Shandong Provincial Natural Science Foundation (ZR2011BQ017), Research Project for the Application Foundation in Qingdao (13−1−4−198−jch), National Natural Science Foundation of China (51102219, 51342008), National High Technology Research and Development Program of China (2010AA09Z203, 2010AA065104), and National Key Technology Support Program (2012BAB15B02).

Notes and references

[a] *Key Laboratory of Marine Chemistry Theory and Technology, Ministry of Education, Ocean University of China, Qingdao 266100, P.R. China; E-mail: tangqunwei@ouc.edu.cn; yuyan@ouc.edu.cn*
[b] *Institute of Materials Science and Engineering, Ocean University of China, Qingdao 266100, P.R. China*
[c] *Qingdao Collaborative Innovation Center of Marine Science and Technology, Ocean University of China, Qingdao 266100, P.R. China*
† Electronic Supplementary Information (ESI) available: Experimental details, photovoltaic and EIS data. See DOI: 10.1039/b000000x/

1 Y. Kuwano, *Adv. Mater.*, 1997, **9**, 295.
2 B. O'Regan and M. Grätzel, *Nature*, 1991, **353**, 737.
3 Y. Luo, D. Li and Q. B. Meng, *Adv. Mater.*, 2009, **21**, 4647.
4 I. Chung, B. Lee, J. Q. He, R. P. H. Chang and M. G. Kanatzidis, *Nature*, 2012, **485**, 486.
5 J.−Y. Lin, C.−Y. Chan and S.−W. Chou, *Chem. Commun.*, 2013, **49**, 1440.
6 X. J. Zheng, J. H. Guo, Y. T. Shi, F. Q. Xiong, W. H. Zhang, T. L. Ma and C. Li, *Chem. Commun.*, 2013, **49**, 9645.
7 M. X. Wu, X. Lin, A. Hagfeldt and T. L. Ma, *Angew. Chem. Int. Ed.*, 2011, **50**, 3520.
8 T. Chen, W. H. Hu, J. L. Song, G. H. Guai and C. M. Li, *Adv. Funct. Mater.*, 2012, **22**, 5245.
9 F. Gong, H. Wang, X. Xu, G. Zhou and Z. S. Wang, *J. Am. Chem. Soc.*, 2012, **134**, 10953.

10 J. H. Wu, Y. M. Xiao, Q. W. Tang, G. T. Yue, J. M. Lin, M. L. Huang, Y. F. Huang, L. Q. Fan, Z. Lan, S. Yin and T. Sato, *Adv. Mater.*, 2012, **24**, 1884.

11 L. C. Chen, J. M. Ting, Y. L. Lee and M. H. Hon, *J. Mater. Chem.*, 2012, **22**, 5596.

12 A. Hilmi, T. A. Shoker, T. H. Ghaddar, *ACS Appl. Mater. Interfaces*, 2014, **6**, 8744.

13 W. Wang, Q. Zhao, H. Li, H. W. Wu, D. C. Zou, D. P. Yu, *Adv. Funct. Mater.*, 2012, **22**, 2775.

14 N. Q. Fu, X. R. Xiao, X. W. Zhou, J. B. Zhang, Y. Lin, *J. Phys. Chem. C*, 2012, **116**, 2850.

15 P. Zhang, C. Wu, Y. Han, T. Jin, B. Chi, J. Pu, L. Jian, *J. Am. Chem. Soc.*, 2012, **95**, 1372.

16 N. Fuke, A. Fukui, R. Komiya, A. Islam, Y. Chiba, M. Yanagida, R. Yamanaka, L. Y. Han, *Chem. Mater.*, 2008, **20**, 4974.

17 J. H. Wu, Z. Lan, J. M. Lin, M. L. Huang, S. C. Hao, T. Sato and S. Yin, *Adv. Mater.*, 2007, **19**, 4006.

18 H. Wang, X. Zhang, F. Gong, G. Zhou and Z. S. Wang, *Adv. Mater.*, 2012, **24**, 121.

19 H. J. Snaith and L. Schmidt−Mende, *Adv. Mater.*, 2007, **19**, 3187.

20 S. S. Yuan, Q. W. Tang, B. B. Hu, C. Q. Ma, J. L. Duan and B. L. He, *J. Mater. Chem. A*, 2014, **2**, 2814.

21 J. H. Wu, Y. Li, Q. W. Tang, G. T. Yue, J. M. Lin, M. L. Huang and L. J. Meng, *Sci. Rep.*, 2014, **4**, 4028.

22 S. Li, Z. Chen, Y. Wang, T. Li, B. Xu and W. Zhang, *J. Electrochem. Soc.*, 2014, **161**, H6.

23 M. Dürr, A. Schmid, M. Obermaier, S. Rosselli, A. Yasuda and G. Nelles, *Nat. Mater.*, 2005, **4**, 607.

24 N. Q. Fu, Y. Y. Fang, Y. D. Duan, X. W. Zhou, X. R. Xiao and Y. Lin, *ACS Nano*, 2012, **6**, 9596.

25 L. Gan, S. Rudi, C. H. Cui and P. Strasser, *ChemCatChem*, 2013, **5**, 2691.

26 K. Suárez−Alcántara and O. Solorza−Feria, *Fuel Cells*, 2010, **10**, 84.

27 B. L. He, X. Meng and Q. W. Tang, *ACS Appl. Mater. Interfaces*, 2014, **6**, 4812.

28 T. Y. Huang, C. W. Kung, H. Y. Wei, K. M. Boopathi, C. W. Chu and K. C. Ho, *J. Mater. Chem. A*, 2014, **2**, 7229.

29 T. Daeneke, A. J. Mozer, T. H. Kwon, N. W. Duffy, A. B. Holmes, U. Bach and L. Spiccia, *Energ. Environ. Sci.*, 2012, **5**, 7090.

30 P. Sudhagar, S. Nagarajan, Y. G. Lee, D. Song, T. Son, W. Cho, M. Heo, K. Lee, J. Won and Y. S. Kang, *ACS Appl. Mater. Interfaces*, 2011, **3**, 1838.

31 Y. Tang, X. Pan, C. Zhang, S. Y. Dai, F. Kong, L. Hu and Y. F. Sui, *J. Phys. Chem. C*, 2010, **114**, 4160.

32 Y. M. Xiao, G. Han, Y. Li, M. Li and Y. Chang, *J. Mater. Chem. A*, 2014, **2**, 3452.

33 X. J. Zheng, J. Deng, N. Wang, D. H. Deng, W. H. Zhang and X. H. Bao, C. Li, *Angew. Chem. Int. Ed.*, 2014, **53**, 1.

34 C. J. Yang, Y. J. Chang, M. Watanabe, Y. S. Hon and T. J. Chow, *J. Mater. Chem.*, 2012, **22**, 4040.

35 M. K. Wang, A. M. Anghel, B. Marsan, N. C. Ha, N. Pootrakulchote, S. M. Zakeeruddin and M. Grätzel, *J. Am. Chem. Soc.*, 2009, **131**, 15976.

36 A. Hanch and A. Georg, *Electrochim. Acta*, 2001, **46**, 3457.

37 X. X. Chen, Q. W. Tang, B. L. He, L. Lin, L. M. Yu, *Angew. Chem. Int. Ed.*, 2014, **53**, 10799.

38 Y. Y. Duan, Q. W. Tang, B. L. He, R. Li and L. M. Yu, *Nanoscale*, 2014, **6**, 12601.